Phosphorylation of Serine 264 Impedes Active Site Accessibility in the E1 Component of the Human Pyruvate Dehydrogenase Multienzyme Complex‡

Franziska Seifert,[§,||] Ewa Ciszak,[||,⊥] Lioubov Korotchkina,[@] Ralph Golbik,[§] Michael Spinka,[§] Paulina Dominiak,[⊥] Sukhdeep Sidhu,[@] Johanna Brauer,[§] Mulchand S. Patel,*[,@] and Kai Tittmann*[,§]

Institut für Biochemie und Biotechnologie, Martin-Luther-Universität Halle-Wittenberg, Kurt-Mothes-Strasse 3, 06120 Halle/Saale, Germany, Laboratory for Structural Biology at the National Space Science and Technology Center, University of Alabama in Huntsville, Huntsville, Alabama 35899, and Department of Biochemistry, School of Medicine and Biomedical Sciences, State University of New York, Buffalo, New York 14214

Received January 16, 2007; Revised Manuscript Received March 22, 2007

ABSTRACT: At the junction of glycolysis and the Krebs cycle in cellular metabolism, the pyruvate dehydrogenase multienzyme complex (PDHc) catalyzes the oxidative decarboxylation of pyruvate to acetyl-CoA. In mammals, PDHc is tightly regulated by phosphorylation−dephosphorylation of three serine residues in the thiamin-dependent pyruvate dehydrogenase (E1) component. In vivo, inactivation of human PDHc correlates mostly with phosphorylation of serine 264, which is located at the entrance of the substrate channel leading to the active site of E1. Despite intense investigations, the molecular mechanism of this inactivation has remained enigmatic. Here, a detailed analysis of microscopic steps of catalysis in human wild-type PDHc-E1 and pseudophosphorylation variant Ser264Glu elucidates how phosphorylation of Ser264 affects catalysis. Whereas the intrinsic reactivity of the active site in catalysis of pyruvate decarboxylation remains nearly unaltered, the preceding binding of substrate to the enzyme's active site via the substrate channel and the subsequent reductive acetylation of the E2 component are severely slowed in the phosphorylation variant. The structure of pseudophosphorylation variant Ser264Glu determined by X-ray crystallography reveals no differences in the three-dimensional architecture of the phosphorylation loop or of the active site, when compared to those of the wild-type enzyme. However, the channel leading to the active site is partially obstructed by the side chain of residue 264 in the variant. By analogy, a similar obstruction of the substrate channel can be anticipated to result from a phosphorylation of Ser264. The kinetic and thermodynamic results in conjunction with the structure of Ser264Glu suggest that phosphorylation blocks access to the active site by imposing a steric and electrostatic barrier for substrate binding and active site coupling with the E2 component. As a Ser264Gln variant, which carries no charge at position 264, is also selectively deficient in pyruvate binding and reductive acetylation of E2, we conclude that mostly steric effects account for inhibition of PDHc by phosphorylation.

PDHc[1] catalyzes the irreversible conversion of pyruvate, coenzyme A, and NAD^+ into CO_2, NADH, and acetyl-CoA, the latter serving as the main precursor for the Krebs cycle and the biosynthesis of fatty acids and steroids (*1*, *2*). With a molecular mass of a few megadaltons, PDHc is the largest and one of the most complex multienzyme systems known (*3*). In mammals, this complex is comprised of four major components: the thiamin diphosphate (ThDP)-dependent pyruvate dehydrogenase (E1), the dihydrolipoamide transacetylase (E2) containing covalently bound lipoyl groups, the flavoenzyme lipoamide dehydrogenase (E3), and the E3-binding protein (E3BP). In addition, mammalian PDHc also contains a family of four pyruvate dehydrogenase kinases (PDKs) and two pyruvate dehydrogenase phosphatases (PDPs), which control the activity of the complex by reversible phosphorylation (*4*). The catalytic sequence (Figure 1A) of PDHc commences in the E1 component, which catalyzes in a series of microscopic steps the decarboxylation of pyruvate and the acetylation of a visiting lipoamide "swinging arm" of the E2 component, thereby coupling catalysis of E1 and E2 in a synchronized manner. As a short-term regulation, reversible phosphorylation of three serine residues of the E1 α-subunit controls the activity of the enzyme complex. In human PDHc, the subject of our studies here, phosphorylation of Ser264 (denoted as site 1) appears to confer in vivo inactivation as phosphorylation of this site completely abolishes activity of the complex, whereas

‡ The refined model and structure factors for PDHc-E1 Ser264Glu have been deposited in the Research Collaboratory for Structural Biology as PDB entry 2OZL.

* To whom correspondence shall be addressed. E-mail: kai.tittmann@biochemtech.uni-halle.de and mspatel@buffalo.edu. Phone: ++49-345-5524887. Fax: ++49-345-5527014.

§ Martin-Luther-Universität Halle-Wittenberg.

|| These authors contributed equally to this study.

⊥ University of Alabama in Huntsville.

@ State University of New York.

[1] Abbreviations: PDHc, pyruvate dehydrogenase multienzyme complex; PDHc-E1, E1 component of PDHc; MAP, methylacetylphosphonate; ThDP, thiamin diphosphate; LThDP, 2-lactyl-ThDP; HEThDP, 2-(1-hydroxyethyl)ThDP; PLThDP, 2-phosphonoLThDP; PDK, pyruvate dehydrogenase kinase; PDP, pyruvate dehydrogenase phosphatase.

10.1021/bi700083z CCC: $37.00
Published on Web 05/03/2007

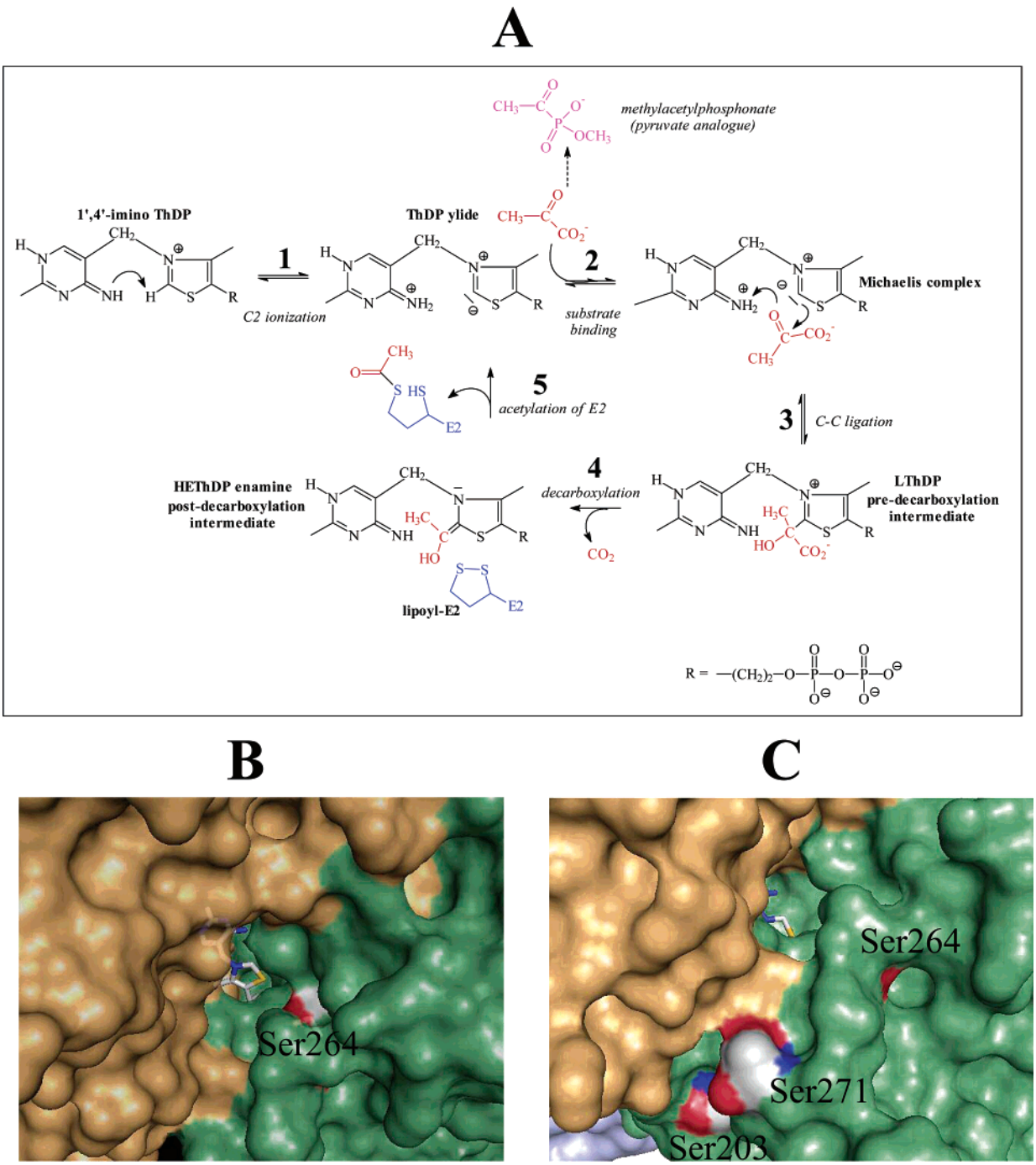

FIGURE 1: Mechanism and regulation sites of the human pyruvate dehydrogenase (E1) component. (A) Sequence of microscopic catalytic steps in E1 with identified intermediates. (B) Surface view (transparent) of the substrate channel in E1 leading to the active site with the cofactor ThDP and the side chain of Ser264 indicated. The corresponding α- and β-subunits are colored individually. (C) Surface view (opaque) of E1 showing the active site channel, the cofactor ThDP, and regulation sites 1 (Ser264), 2 (Ser271), and 3 (Ser203). For clarity, the diphosphate moiety of ThDP was deliberately omitted from panel B.

PDHc with phosphorylated site 2 (Ser271) or 3 (Ser203) retains moderate catalytic activity (*5*). In the X-ray crystal structure(*6*), Ser264 is positioned at the entrance of the substrate channel with the hydroxyl moiety of the side chain pointing right into the channel (Figure 1B). Ser271 and Ser203 are located farther from the active site (Figure 1C). The mechanism by which phosphorylation inactivates PDHc or related 2-oxo acid dehydrogenase complexes has been controversially discussed. Earlier studies suggested that catalysis in E1 might be affected (*7*, *8*). On the other hand, a kinetic analysis of isolated human PDHc-E1 revealed that site 1 phosphorylation or pseudophosphorylation (replacement of serine with glutamate) appeared to have an only small effect on catalysis when monitored in commonly used steady-state assays of model E1 reactions (*5*). Thus, it had been concluded that active site coupling of E1 and E2 is impaired as also suggested for the related branched chain keto acid dehydrogenase complex (*9*). Recent transient kinetics studies on human PDHc-E1 have shown (*10*), however, that all microscopic catalytic steps are several orders of magnitude faster than the overall reaction rate of E1 determined in steady-state assays, which make use of

Table 1: Microscopic Rate and Equilibrium Constants (see Figure 1A) of the Activated Site in Human Wild-Type PDHc and Variants Ser264Glu and Ser264Gln[a]

microscopic rate and equilibrium constants of elementary steps of catalysis	wild-type PDHc-E1	PDHc-E1 variant Ser264Glu	PDHc-E1 variant Ser264Gln
step 1			
ionization rate constant of C2 of ThDP, k_{obs} (s^{-1})	51 ± 15	71 ± 10	18 ± 9
step 2			
on-rate for pyruvate analogue MAP, k_{on} (M^{-1} s^{-1})	60 ± 1	2.5 ± 0.1	0.9 ± 0.1
off-rate for pyruvate analogue MAP, k_{off} (s^{-1})	0.0027 ± 0.0001	0.00255 ± 0.00001	0.012 ± 0.001
dissociation constant for MAP (kinetics), K_{app} (mM)	0.045	1.02	13.3
dissociation constant for MAP (CD titration), K_{app} (mM)	0.046 ± 0.004	0.941 ± 0.070	1.513 ± 0.181
step 3			
net rate constant of LThDP formation, k' (s^{-1})	2.3 ± 0.5[b]	0.033 ± 0.009[b]	0.023 ± 0.002[b]
step 4			
net rate constant of LThDP decarboxylation, k' (s^{-1})	5.1 ± 1.3	$\gg$step 3	$\gg$step 3
step 5			
reductive acetylation of E2, k (s^{-1})	50−70[c]	no detectable activity	1.5 (3% of residual activity)

[a] Steps 1−4 were analyzed for isolated PDHc-E1, and step 5 in the reconstituted complex was as described in ref *5*. [b] At 25 mM (wild type) and 30 mM pyruvate (variants). Please note that for the variants the observed net rate constant is not maximal at this pyruvate concentration. [c] For PDHc, reductive acetylation of E2 is thought to be rate-limiting for overall catalysis (*11*).

very slow artificial or side reactions. Therefore, these kinetic tools are not suitable for reliably detecting kinetic changes of elementary steps of catalysis (*10*).

Here, we have analyzed microscopic steps of catalysis in wild-type PDHc-E1 and the pseudophosphorylation variant Ser264Glu, which has been previously shown to be a viable model for site 1-phosphorylated E1 alone and in the multienzyme complex (*5*, *9*). Aside from measures of overall activity and E1 model reactions, microscopic rate constants and equilibrium constants were determined for elementary steps of the E1-catalyzed reaction sequence (Figure 1A) encompassing (i) formation of the reactive ThDP C2 carbanion in the active site of E1 (step 1), (ii) the reversible binding of the substrate to and from E1's active site (step 2), (iii) formation of the covalent predecarboxylation intermediate (step 3), (iv) decarboxylation of the adduct (step 4), and (v) reductive acetylation of E2 (step 5) that is considered to be rate-limiting for the overall activity of the active unphosphorylated complex (*11*). In addition to the experiments with the physiological substrate pyruvate, the enzyme was also reacted with the pyruvate analogue methylacetylphosphonate (MAP, Figure 1A) (*12*, *13*). This compound forms a covalent bond with C2 of ThDP similar to that of pyruvate (*14*, *15*), but the adjacent C_α−P bond cannot be cleaved enzymatically (Figure 1A of the Supporting Information). Therefore, catalysis arrests at the predecarboxylation intermediate stage, allowing for a separate kinetic and thermodynamic analysis of the substrate binding sequence (steps 2 and 3 in Figure 1A). Besides the kinetic and thermodynamic analysis of elementary catalytic steps, the X-ray structure of the E1 pseudophosphorylation variant Ser264Glu was determined and compared to that of the wild-type enzyme.

MATERIALS AND METHODS

Protein Production, Reaction Intermediate Analysis, and Chemical Synthesis. Human wild-type PDHc-E1 and the variants Ser264Glu and Ser264Gln were recombinantly produced in *Escherichia coli* M15 cells containing the pQE-9-6HE1α/E1β plasmid. Fermentation of the cells and protein purification were carried out as detailed in ref *10*.

Formation of the reactive C2 carbanion of enzyme-bound ThDP and single-turnover pyruvate decarboxylation by PDHc-E1 were analyzed using chemical quenched-flow/^{1}H NMR spectroscopic methods (*10*, *16*, *17*). For that purpose, 15 mg/mL PDHc-E1 was reconstituted with an equimolar amount of ThDP and 5 mM Mg^{2+} in 0.1 M potassium phosphate buffer (pH 7.6) and 300 mM KCl. Under these conditions and if we take into account the cofactor's dissociation constant of 0.47 μM (wild-type), 0.92 μM (Ser264Glu), or 0.47 μM (Ser264Gln), approximately 95% of the active sites are occupied with ThDP in dynamic equilibrium. Thereafter, the enzyme was mixed with either 99.9% (v/v) D_2O (C2 ionization) or the substrate pyruvate (single-turnover decarboxylation) for defined reaction times in a chemical quenched-flow apparatus (KinTek, Althouse) for reaction times of up to 2000 ms or by manual mixing for longer reaction times followed by acid quench of the reaction, separation of the reaction intermediates, and ^{1}H NMR spectroscopic and kinetic analysis as described in ref *10*.

Table 2: X-ray Crystallographic Statistics for the Human E1 Ser264Glu Variant

data collection	
resolution range (Å)	50−1.90 (2.00−1.90)
space group	$P2_12_12_1$
unit cell dimensions	
a, *b*, *c* (Å)	64.9, 126.4, 190.4
α, β, γ (deg)	90.0
no. of reflections	111312 (9382)
completeness (%)	91.1 (76.6)
redundancies	3.23 (2.3)
R_{sym} (%)[a]	0.11 (0.31)
$I/\sigma(I)$	5.56 (3.61)
refinement statistics[b]	
resolution range (Å)	50.0−1.90 (2.00−1.90)
no. of reflections	106472
R_{cryst}[c]	0.186 (0.218)
R_{free}[d]	0.221 (0.253)
root-mean-square deviation	
bond lengths (Å)	0.005
bond angles (deg)	2.1
dihedral angles (deg)	1.6
improper angles (deg)	3.1

[a] $R_{sym} = \sum|I - \langle I\rangle|/\sum I$, where I is the integrated intensity of a given reflection. [b] The numbers in parentheses are for the highest-resolution shell from 1.90 to 2.00 Å. [c] $R_{cryst} = \sum|F_o - F_c|/\sum F_o$. [d] $R_{free} = \sum|F_o - F_c|/\sum F_o$, where F_o values are test set amplitudes (10.0%) not used in refinement.

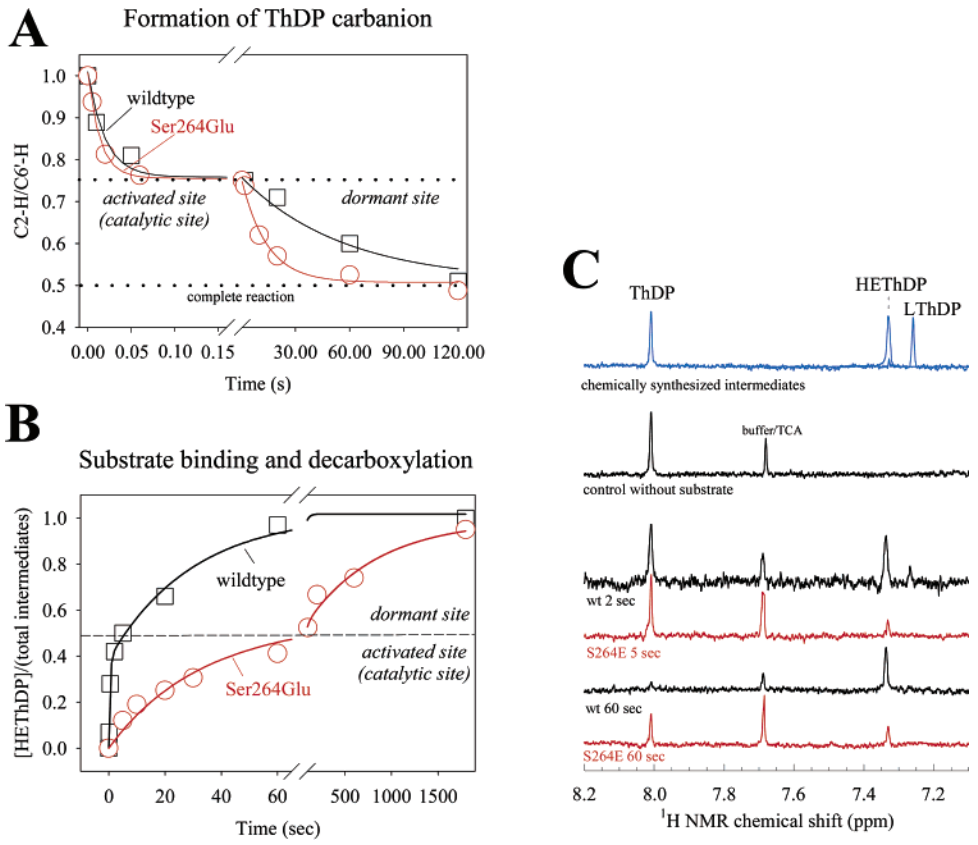

FIGURE 2: Microscopic kinetic analysis of wild-type E1 and pseudophosphorylated E1 (Ser264Glu) by transient quenched-flow/^{1}H NMR spectroscopy. (A) Formation of the reactive ThDP carbanion (step 1 in Figure 1A) monitored by a H−D exchange technique (*16*). (B) Pyruvate decarboxylation in E1 (steps 2−4 in Figure 1A) under single-turnover conditions (*10*, *17*). (C) Selected ^{1}H NMR spectra of isolated reaction intermediates obtained after acid quench of working wild-type E1 and Ser264Glu at different reaction times are shown. Please note that the predecarboxylation intermediate LThDP is exclusively observed in wild-type E1. Kinetic constants are given in Table 1.

For an independent kinetic and thermodynamic analysis of the substrate binding sequence, PDHc-E1 was reacted with the chemically synthesized pyruvate analogue methylacetylphosphonate (MAP). This compound forms a stable predecarboxylation intermediate that gives rise to both a circular dichroism and an absorbance signal centered around 290−295 nm. The apparent dissociation constant of MAP under equilibrium conditions was determined using the circular dichroism signal of the predecarboxylation intermediate after titration of increasing amounts of MAP as a sodium salt to 2 mg/mL enzyme (reconstituted with 0.1 mM ThDP and 1 mM Mg^{2+}) in 0.1 M potassium phosphate buffer (pH 7.6) and 300 mM KCl. The rate constants for binding of MAP to enzyme-bound ThDP were determined by stopped-flow kinetics at 295 nm and an optical path length of 10 mm. PDHc-E1 (at 4 mg/mL, reconstituted with 0.2 mM ThDP and 1 mM Mg^{2+}) in 0.1 M potassium phosphate buffer (pH 7.6) and 300 mM KCl were mixed with various concentrations of MAP (in the same buffer) in a 1:1 ratio at 30 °C. The progress curves that were obtained were fitted to a monoexponential function. In view of the apparent linear dependence of k_{obs} on the analogue concentration, the following equation was used to fit the data:

$$k_{obs} = k_{off} + k_{on}[MAP]$$

where k_{on} is the apparent second-order rate constant for MAP binding and k_{off} the apparent first-order rate constant for dissociation from the enzyme.

Protein Crystallization and Data Collection. Crystals of PDHc-E1 Ser264Glu were grown using a modified protocol developed for wild-type E1 (*18*). Crystallization droplets containing 8−10 mg/mL protein (supplemented with 0.2 mM ThDP and 1 mM Mg^{2+}) in 50 mM potassium phosphate buffer (pH 8.0), 5 mM DTT, 0.1 mM sodium azide, 100 mM NaSCN, and 6−8% PEG 3350 (v/v) were equilibrated over a reservoir solution containing 14−18% PEG 3350, 0.1 mM sodium azide, and 200 mM NaSCN, all in 50 mM potassium phosphate (pH 8.0). A crystal with dimensions of 0.3 mm × 0.2 mm × 0.08 mm was soaked for several seconds in cryoprotectant consisting of the reservoir solution and glycerol mixed in a 3:1 (v/v) ratio. The crystal was flash-frozen in liquid nitrogen and transferred to an X-ray diffractometer. Data were collected at Argonne National Laboratory, beamline BM19 at 100 K, and processed with HKL2000 (*19*) in space group $P2_12_12_1$ with the E1-Ser264Glu tetramer in the asymmetric unit and the following cell dimensions: a = 64.9 Å, b = 126.4 Å, and c = 190.4 Å. The diffraction data extended to a resolution of 1.67 Å.

Structure Determination. The $\alpha_2\beta_2$ structure of PDHc-E1 Ser264Glu was determined using the methods of isomorphous molecular replacement using the structure of human E1 (PDB entry 1NI4) as a search model (*6*). The initial model was subjected to rigid body refinement using CNS (*20*). After several cycles of model building and refitting using XtalView (*21*), all 1380 residues of the Ser264Glu protein and four

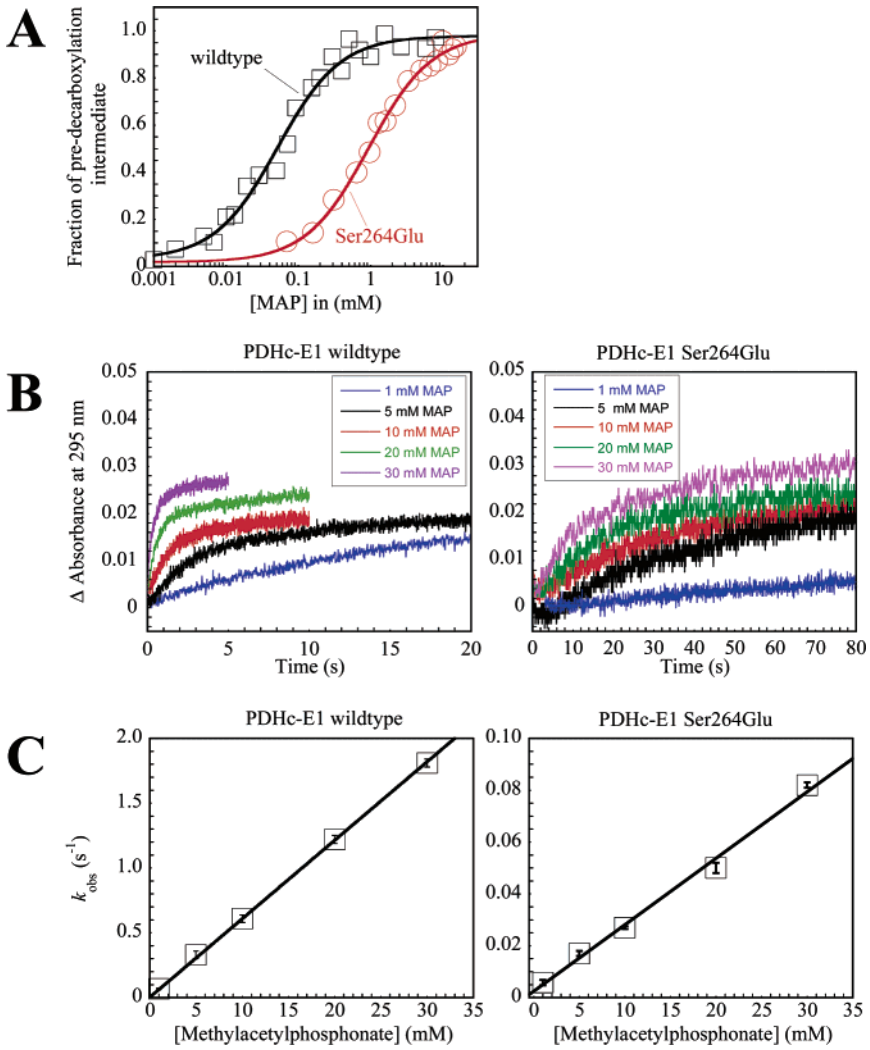

FIGURE 3: Transient kinetic and CD spectral thermodynamic analysis of the substrate binding sequence (steps 2 and 3 in Figure 1A) in wild-type and pseudophosphorylated E1 employing methylacetylphosphonate (MAP) as a substrate analogue not undergoing decarboxylation. (A) Normalized binding plots for binding of MAP to wild-type E1 and the variant Ser264Glu as analyzed by CD spectroscopy. CD spectra are shown in the Supporting Information. (B) Formation of the stable predecarboxylation intermediate analogue analyzed by stopped-flow kinetics. (C) Dependence of the observed rate constants obtained in panel B on the substrate analogue concentrations. Stopped-flow transients were fitted to a monoexponential function. Measurements were carried out in triplicate, and the corresponding error bars are indicated. Kinetic and thermodynamic constants are given in Table 1.

additional residues resulting from cloning, one at the N-terminus of each subunit, were located. The experimental as well as the simulated annealing omit maps clearly showed the presence of Glu264 in the structure. Finally, two ThDP molecules, two Mg^{2+} ions, two K^+ ions, and 757 water molecules were added, and refinement continued to convergence using all data to 1.9 Å resolution. The final R_{cryst} and R_{free} values are 0.186 and 0.221, respectively, with 90.1% of the residues in the most favored regions of the Ramachandran plot and the remaining ones in the additional allowed regions. In each case, those residues have well-defined electron density. The final statistics of data collection and refinement are listed in Table 2.

Figures were prepared using either XtalView (*21*) or Pymol (DeLano Scientific, http://www.pymol.org).

RESULTS

In the fully reconstituted human multienzyme PDH complex, site 1 phosphorylation or pseudophosphorylation completely abolishes overall activity whereas cofactor binding is not affected (*5*). One can surmise that any microscopic step at E1 (steps 1−5 in Figure 1A) could be a potential regulation point of the enzymatic reaction because all corresponding nonenzymic reactions are at least 6 orders of magnitude slower. If specific catalysis provided by the enzyme for any of those steps would be impaired or abolished by phosphorylation, overall catalysis will be rate-limited by this particular step (*22*).

Transient Chemical Quench/^{1}H NMR Kinetic Studies of Microscopic Steps of Catalysis. First, we analyzed the ability of wild-type E1 and the variant Ser264Glu to catalyze the initial formation of the reactive thiamin C2 carbanion (step 1) using a H−D exchange chemical quench/NMR technique (*16*). Studies on the related enzyme pyruvate decarboxylase from yeast, which is subject to homotropic substrate activation triggered at a regulatory site some 23 Å from the active site, have shown that catalysis of thiamin enzymes can be regulated at this initial stage by activating and deactivating the cofactor (*16*). However, our kinetic studies on PDHc clearly show that cofactor activation in the catalytically active

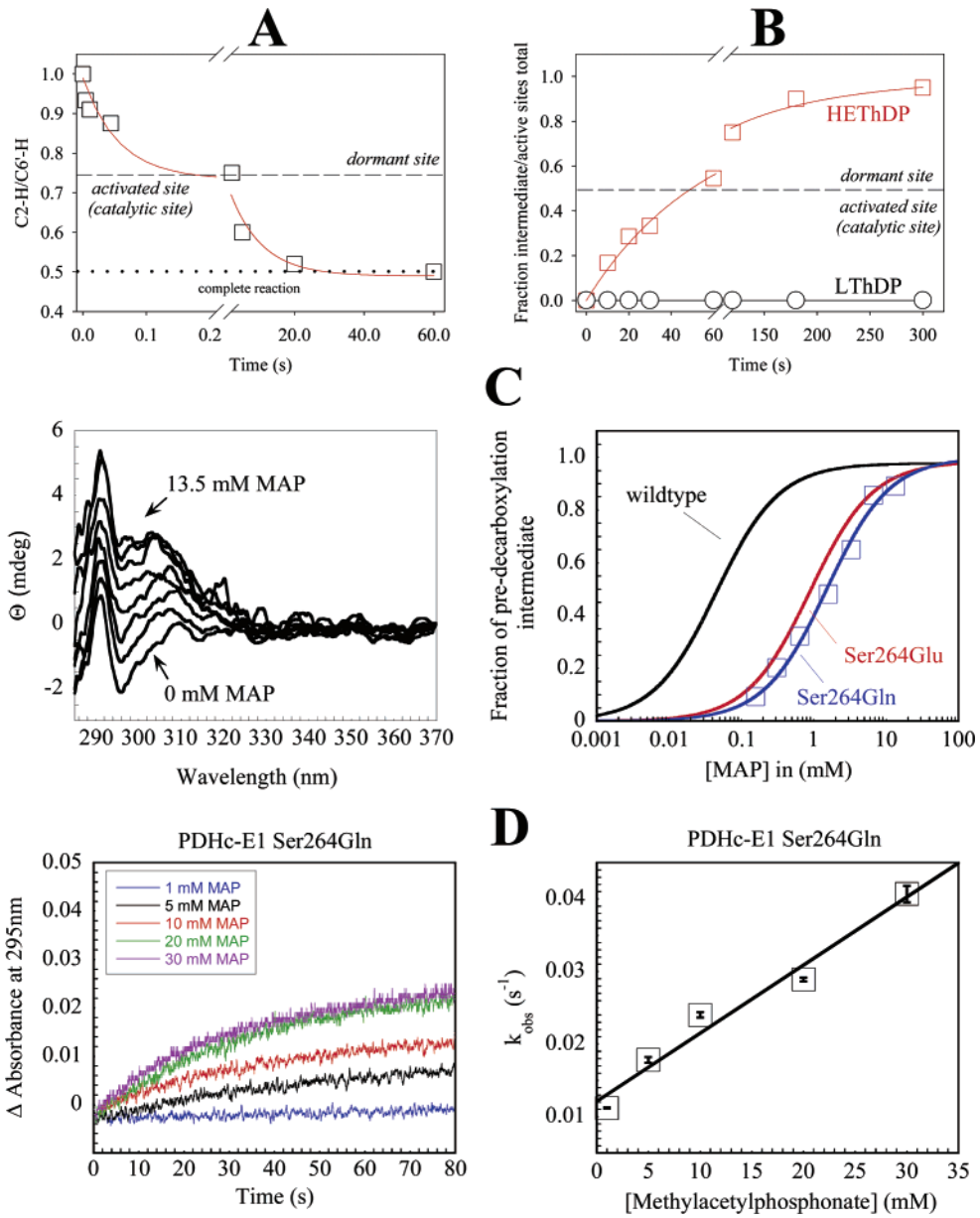

FIGURE 4: Kinetic and thermodynamic analysis of elementary catalytic steps of the PDHc-E1 Ser264Gln variant (a pseudophosphorylation variant with no charge at position 264) by transient NMR and stopped-flow kinetics, and CD spectral analysis (see the text). (A) Cofactor activation. (B) Pyruvate decarboxylation under single-turnover conditions. (C) CD spectral titration using the pyruvate analogue MAP (left) and normalized binding plot (right). (D) Transients of MAP binding (left) and dependence of k_{obs} on the MAP concentration (right). The kinetic and thermodynamic constants are summarized in Table 1.

site of PDHc-E1 is virtually unaffected by pseudophosphorylation (Figure 2A and Table 1), thus ruling out deactivation of ThDP as accounting for inactivation of PDHc. Notably, the two active sites in $\alpha_2\beta_2$-type PDHc-E1 are chemically and functionally nonequivalent and are termed a "dormant site" and an "activated site" with the latter solely accounting for catalysis (*10*, *23*).

Next, we kinetically analyzed the reaction of isolated E1 with pyruvate using transient chemical quench/NMR methods (*17*). In the absence of all other components of PDHc, E1 only catalyzes a single-turnover reaction comprising steps 1−4 in Figure 1A with the 2-hydroxyethyl-ThDP (HEThDP) enamine as a final intermediate and the predecarboxylation adduct 2-lactyl-ThDP (LThDP) as a transient intermediate. We could detect both intermediates in wild-type E1 and demonstrated that at saturating pyruvate concentrations the unimolecular forward net rate constants of addition of pyruvate from a docking site to C2 of ThDP (step 3) and decarboxylation (step 4) can be assessed (*10*). Contrary to these results, we could not detect the predecarboxylation intermediate in Ser264Glu PDHc-E1, indicating that decarboxylation is clearly faster than the preceding steps of catalysis (steps 2 and 3) and not rate-limiting (Figure 2B,C). Also, the apparent rate constant of enamine formation in the activated site is slowed 70-fold when compared to that of wild-type E1 (Table 1) and, even above 30 mM pyruvate, remains dependent on the substrate concentration, suggesting the bimolecular substrate association with the enzyme (step 2) to be at least partially rate-limiting for catalysis (Figure 2 of the Supporting Information). Therefore, we conclude that unimolecular steps of catalysis in the active site (steps 3 and 4) are not largely affected by pseudophosphorylation which rather seems to kinetically block binding of substrate to the active site.

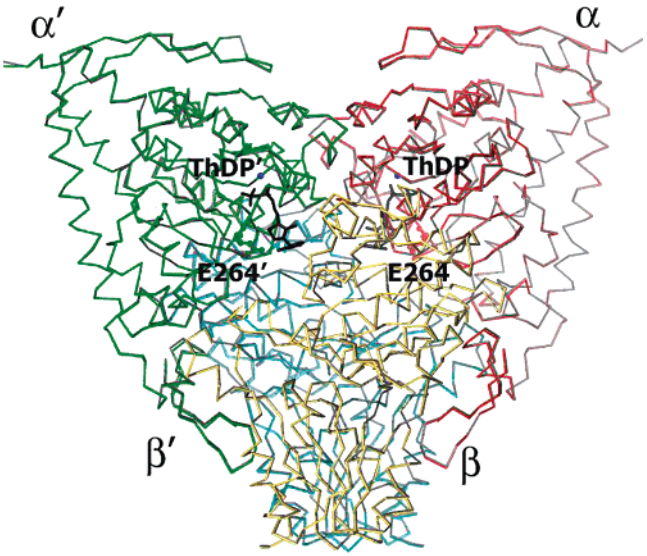

FIGURE 5: Superposition of the structures of wild-type E1 and variant Ser264Glu after least-squares alignment. The black lines represent the C_α trace of the wild-type protein. For the variant, all four corresponding subunits are colored individually with the α-subunits colored green and red and the *β*-subunits yellow and blue. ThDP molecules are colored black, and Mg^{2+} and Glu264 side chains are shown as spheres.

Transient Stopped-Flow Kinetics and Thermodynamic Studies of Substrate Binding Using a Nondecarboxylating Substrate Analogue. To analyze the substrate binding sequence (bimolecular association with the enzyme and unimolecular ligation to ThDP) separately, we reacted PDHc-E1 with the pyruvate analogue methylacetylphosphonate (MAP), which forms a stable predecarboxylation intermediate analogue that gives rise to a circular dichroism (*10*) and an absorbance signal centered around 290 nm (Figure 1 of the Supporting Information). The former signal can be used to determine the overall equilibrium constant for both binding steps (steps 2 and 3 in Figure 1A) in a presumably two-step reversible reaction mechanism:

$$\text{PDHc-E1} + \text{substrate} \overset{K_1}{\leftrightarrows} \text{PDHc-E1*substrate (Michaelis complex)} \overset{K_2}{\leftrightarrows} \text{predecarboxylation intermediate}$$

As shown in Figure 3A, the apparent dissociation constant of MAP under equilibrium conditions is 20-fold increased for pseudophosphorylated E1 (K_{app} = 1 mM) when compared to that of wild-type E1 (K_{app} = 0.047 mM). This result clearly indicates that binding of substrate to E1's active site is severely affected by pseudophosphorylation. Notably, this tremendous effect can be detected over the whole pH range that was tested (pH 6.5−8.0) for human PDHc-E1 and accounts at pH 7.0 for an as much as 30−40-fold increase in the substrate's equilibrium constant in the phosphorylation variant (K_{app} = 2.45 ± 0.37 mM) compared to that of the wild-type enzyme (K_{app} = 78.18 ± 6.32 *μ*M) (data not shown). The CD spectroscopic data do not allow us to draw reliable conclusions concerning which microscopic step of the binding sequence is affected by pseudophosphorylation. Therefore, we analyzed the binding of MAP to the enzyme by transient stopped-flow kinetics using the absorbance signal of the predecarboxylation intermediate analogue. At high substrate analogue concentrations, the reaction in wild-type

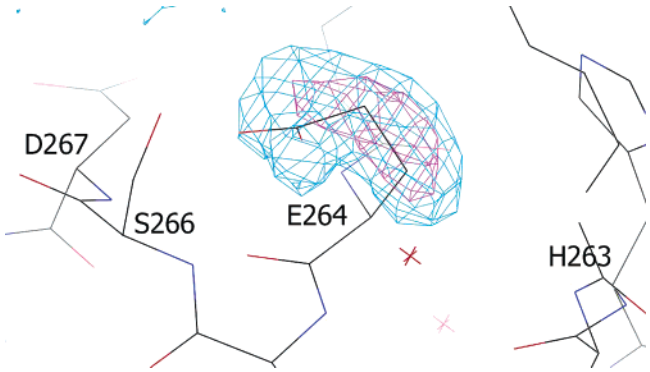

FIGURE 6: Simulated annealing $F_o - F_c$ omit map of residue 264 in PDHc-E1 Ser264Glu calculated prior to inclusion of the glutamate side chain at position 264 in the refinement. The map is contoured at 3*σ* (blue lines) and 5*σ* (purple lines).

E1 has a half-time of less than 500 ms (Figure 3B). By contrast, the reaction of the variant under similar conditions has a half-time of approximately 12 s. As observed for both the wild-type enzyme and the variant, the apparent rate constant depends on the substrate analogue concentration in a linear manner, implying that the bimolecular association kinetically determines the overall rate (Figure 3C). Therefore, the data allow us to extract the apparent second-order on-rate constant of the substrate (binding to the active site) and the apparent first-order off-rate (dissociation from the active site). The analysis reveals the off-rate constant to be virtually the same for the wild type and the phosphorylation variant, whereas the on-rate constant is approximately 25-fold smaller for the variant, resulting in a residual activity of only a few percent after phosphorylation under substrate subsaturation conditions (Table 1). The equilibrium constants calculated from the kinetic experiments ($K_D = k_{off}/k_{on}$) are similar to those obtained in the thermodynamic studies. This fact and the observation of only one relaxation time are consistent with a simple reversible one-step mechanism of MAP binding. That notwithstanding, we cannot rule out a two-step mechanism with the second step being markedly faster than the first. Alternatively, a two-step mechanism in terms of a rapid pre-equilibrium preceding the rate-determining second step (unimolecular forward and reverse) can also be envisioned. In view of the linear dependence of k_{obs} on the MAP concentration, this would require, however, that the dissociation constant (pre-equilibrium) of the substrate analogue be ≫30 mM. A pre-equilibrium mechanism with a dissociation constant for MAP of <30 mM can be excluded because a hyperbolic dependence of k_{obs} on the substrate analogue concentration would be expected in that case for the large concentration range of MAP (0−30 mM) covered in the kinetic experiments. Independent of the kinetic model and even by considering a fast pre-equilibrium, the kinetic data suggest that unimolecular steps of catalysis are not largely affected by pseudophosphorylation but rather binding of the substrate to the active site (see Mathematical Appendix).

Is Inhibition by Phosphorylation a Size- or Charge-Related Effect? Studies on the "Uncharged Phosphorylation Variant" Ser264Gln. By theory, both steric and electrostatic effects of the phosphoserine/glutamate side chains can be envisioned to account for PDHc inhibition as a phosphorylation of Ser264 or its replacement with glutamate makes the side chain bigger and introduces a negative charge. To dissect

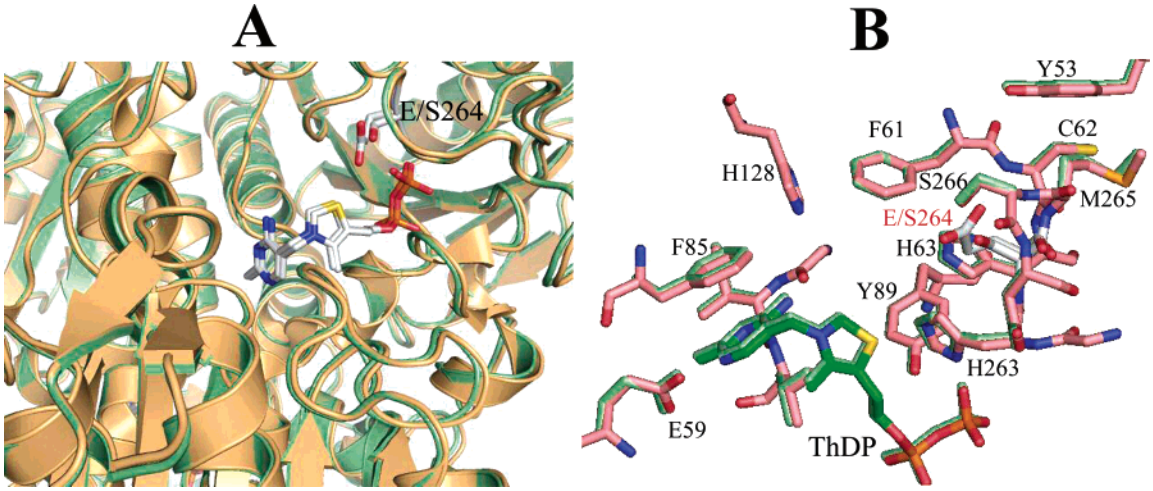

FIGURE 7: (A) Superposition of the phosphorylation loop in human wild-type PDHc (orange) and pseudophosphorylation variant Ser264Glu (green). The cofactor ThDP and the side chains of residues Ser264 (wild type) and Glu264 (variant) are indicated. (B) Superposition of the active sites in human wild-type PDHc and pseudophosphorylation variant Ser264Glu (green) showing the cofactor ThDP and selected amino acid side chains. Residue 264 in each case is highlighted.

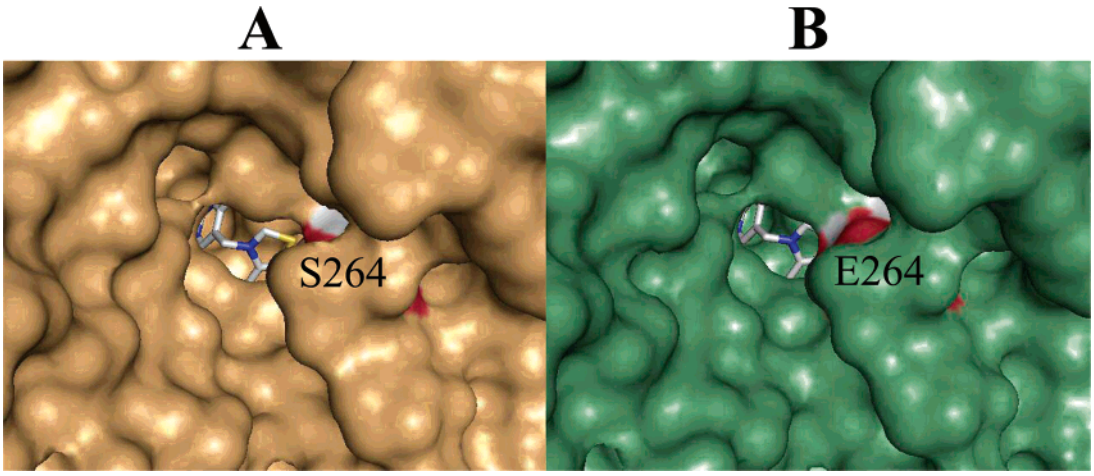

FIGURE 8: Structural comparison of the active site accessibility in wild-type PDHc-E1 (A) and pseudophosphorylation variant Ser264Glu (B) in surface representation. The cofactor ThDP is shown in stick representation, and the side chains of residue 264 are highlighted. The structures suggest a partially obstructed substrate channel in the variant.

whether steric hindrance and/or electrostatic repulsion of phosphoSer264 or Glu264 causes inhibition, we have analyzed the kinetics and thermodynamics of elementary catalytic steps of a Ser264Gln variant where the side chain of residue 264 is the same size as that of the pseudophosphorylation variant Ser264Glu but carries, as opposed to the latter, no charge.

Unimolecular reaction steps such as cofactor activation and decarboxylation of the LThDP intermediate are, within experimental uncertainty, not largely affected in PDHc-E1 Ser264Gln when compared to wild-type PDHc-E1 and Ser264Glu (Figure 4 and Table 1). On the contrary, bimolecular binding of pyruvate and that of the pyruvate analogue MAP are as severely affected as that observed for the Ser264Glu variant, suggesting that predominantly steric effects cause a slowed substrate binding in the phosphorylated enzyme. There is some residual activity of Ser264Gln in the overall PDHc assay not seen for the Ser264Glu variant (Table 1). From this observation, it can be concluded that the blocked reductive acetylation of E2 in the phosphorylated or pseudophosphorylated enzyme is, aside from steric hindrance, also caused by electrostatic repulsion between phosphoSer264/Glu264 and E2.

X-ray Structural Analysis of the Ser264Glu Pseudophosphorylation Variant. The E1 Ser264Glu crystal structure resembles the structure of wild-type E1 (*6*). As shown in Figure 5, the protein is composed of four subunits, namely, α, α', β, and β', that are arranged in a tetrahedral manner. All 1380 C_α atoms of the four subunits in the variant are structurally equivalent to those of the wild-type enzyme. The binding and conformation of the ThDP cofactor and the binding of Mg^{2+} ions are also similar in both enzymes. Subsequent least-squares alignment of these structures gave an overall root-mean-square deviation (rmsd) of 0.57 Å corresponding to small shifts in the relative organization of domains, which form the intact subunits. Residue Glu264 could be identified in the structure and exhibits defined electron density (Figure 6).

In the structure of human PDHc-E1, Ser264 residues of the α-subunits are located in long loops, each originating from an α-helix at Ser246 and ending at Thr274, the first residue of a β-strand. In the E1 Ser264Glu structure, these loops remain similar (Figure 7A). This includes the χ_1 torsion angle of the mutated residue at position 264, indicating that the C^β and C^γ atoms of the glutamate side chain would take the place of C^β and O^γ, if it were in wild-type E1. In both

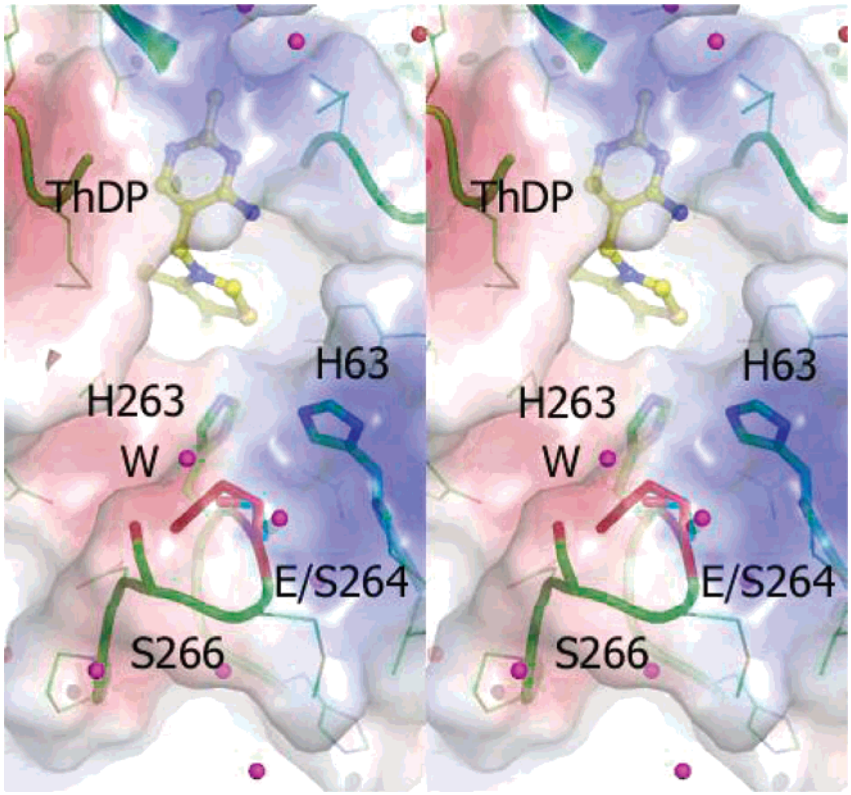

FIGURE 9: Stereodrawing representing the vicinity of the mutation site 264 in the α-subunits with electrostatic properties indicated. The drawing is centered on the C2 atom of ThDP viewed down the substrate binding channel. The mutation site 264 is a superposition of structures of wild-type serine and the variant glutamate showing the contacts that both side chains make with Ser266 and with water molecules (W) in their respective crystal structures. The proximity of the mutation site to His263 of the α-subunit and His63 of the *β*-subunit indicates that that substitution of Ser for Glu is associated with electrostatic changes in this region. Shades of red and blue represent the range of electrostatic charge on the surface of the channel from red being negative to blue being positive.

structures, residue 264 forms a contact with Ser266 (Figure 6). Glu264 adopts a curled conformation with its carboxyl O^{ϵ} atoms reaching to not only O^{γ} of Ser266 but also the amino nitrogen of Ser266 (2.65 and 2.70 Å, respectively). This is a rarely reported conformation of the side chain ($\chi_1 = 47°$, $\chi_2 = 67°$, and $\chi_3 = -92°$) that exhibits strong and specific interactions with the immediate surrounding. The most common rotamers (*24*) of Glu264 would bring the side chain into the space of the substrate channel and closer to His263 of α-subunits and His63 of *β*-subunits (Figure 3 of the Supporting Information). In addition, carboxyl oxygen atoms form hydrogen bonds with two nearby water molecules. The side chain of Glu264 in this rare conformation is well-defined in the crystal. Also, the geometry of all active site residues is virtually unchanged in the pseudophosphorylation variant (Figure 7B). An analysis of the surfaces of the two enzymes reveals, however, that the substrate channel leading to the active site is partially obstructed in the pseudophosphorylated enzyme when compared to the wild-type enzyme (Figure 8). In addition to this steric effect, pseudophosphorylation results in a change in the electrostatic charge at the entrance to the catalytic site of ThDP to strongly negative (Figure 9).

DISCUSSION

Our kinetic and thermodynamic studies on wild-type PDHc-E1 and PDHc-E1 in the pseudophosphorylated state have shown that both binding of the substrate pyruvate to E1's active site and reductive acetylation of the E2 component are severely impaired. By contrast, acid/base and covalent catalysis in the active site such as ThDP cofactor ionization and decarboxylation of the predecarboxylation intermediate LThDP are not largely affected. In line with this, the active site geometry is found to be unaltered in the X-ray structure of the pseudophosphorylated Ser264Glu variant. The overall structure of the enzyme and that of the phosphorylation loop remain unchanged upon phosphorylation. As opposed to this finding, an order-to-disorder transition of the conserved phosphorylation loop has been described for the related E1 component of the human branched chain α-keto acid dehydrogenase complex, resulting in an abolished coupling of its E1 and E2 components (*9*). In human PDHc, both steric and electrostatic factors appear to cause the apparent inhibition of pyruvate and E2 binding as a result of phosphorylation. A comparison of the wild-type structure and that of Ser264Glu provided evidence that the substrate channel is clearly narrowed upon pseudophosphorylation and is the primary conformation following phosphorylation. The steps of phosphorylation and dephosphorylation likely require a disorder transition to make the serine and phosphoserine available for the PDK and PDP, respectively. However, it remains to be determined whether such a disordered conformation makes a significant contribution when E1 is not interacting with the regulatory enzymes. Also, phosphorylation is accompanied by an apparent change in the local electrostatic properties of the substrate funnel. However, electrostatic repulsion appears not to be the major determinant of phosphorylation-mediated inhibition as a Ser264Gln substitution (a pseudophosphorylated variant with no charge at position 264) results in an enzyme with a

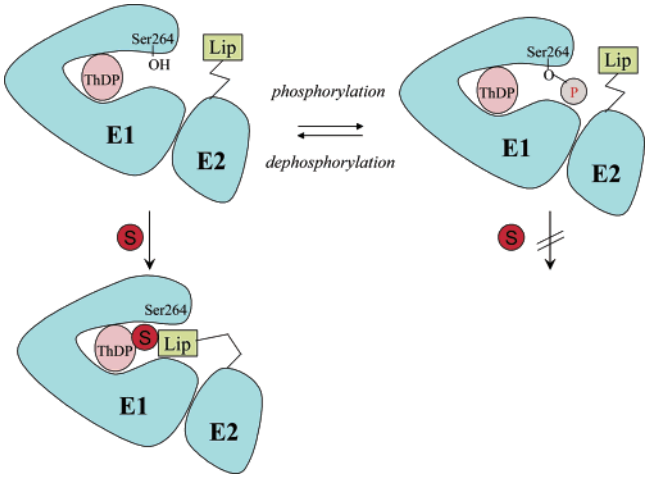

FIGURE 10: Suggested regulation mechanism of human PDHc. The impaired active site accessibility impedes binding of both the substrate pyruvate and the lipoamide swinging arm of the E2 component to E1's active site.

residual activity of just a few percent in the overall activity of the PDHc (*5*) and a 50−100-fold slowed binding of pyruvate or the pyruvate analogue when analyzed by transient NMR and stopped-flow kinetics. On the basis of the kinetic, thermodynamic, and structural data described in this study, we suggest that phosphorylation of Ser264 in human PDHc impairs active site accessibility by mounting a barrier at the entrance of the substrate channel, resulting in smaller on-rates for both pyruvate binding and binding of E2 (Figure 10). Hence, phosphorylation or dephosphorylation starts to control the mode of action of human PDHc at the earliest stage of catalysis, namely pyruvate binding, thereby avoiding undesired side reactions of pyruvate-derived intermediates in PDHc-E1 and a loss of synchronization of E1−E2 coupling. This study provides a molecular mechanism of PDHc regulation by phosphorylation. Whether similar mechanisms may hold true for related complexes such as the branched chain α-keto acid dehydrogenase complex, where the catalytic properties of isolated wild-type E1 and E1 in the phosphorylated state could only be assessed in artificial steady-state assays not suitable for the analysis of elementary steps of catalysis, remains to be determined by the kinetic and thermodynamic tools used in this study.

MATHEMATICAL APPENDIX

The formation of 2-α-phosphonolactyl-ThDP (see Figure 1A of the Supporting Information) proceeds presumably via a two-step reversible mechanism:

$$\underbrace{\text{E}-\text{ThDP}}_{\text{A}} + \underbrace{\text{MAP}}_{\text{M}} \underset{k_{-S}}{\overset{k_S}{\rightleftharpoons}} \underbrace{\text{E}-\text{ThDP}\cdot\text{MAP}}_{\text{B}} \underset{k_{-1}}{\overset{k_1}{\rightleftharpoons}} \underbrace{\text{E}-\text{PLThDP}}_{\text{C}} \qquad \text{(A1)}$$

K_S K_1

At equilibrium, the fraction $[C]/[A]_0$ is given by

$$\frac{[C]}{[A]_0} = \frac{\alpha[M]_0}{K_{app} + [M]_0} \qquad \text{(A2)}$$

with

$$\alpha = (1 + K_1)^{-1} \qquad \text{(A3)}$$

$$K_{app} = \frac{K_S K_1}{1 + K_1} \qquad \text{(A4)}$$

Values of $[C]/[A]_0$ have been determined by CD measurements (Figure 3A) at various MAP concentrations. The data were evaluated according to eq A2. The following values were obtained: $K_{app}^{WT} = 0.047$ mM and $K_{app}^{Var} = 1.0$ mM. Kinetically, the formation of 2-α-phosphonolactyl-ThDP is described by

$$\frac{d[C]}{dt} = k_1[B] - k_{-1}[C] \qquad \text{(A5)}$$

In line with the assumption of a fast pre-equilibration of the initial binding step in sequence A1 which can be made in view of the binding of the native substrate pyruvate, [B] might be approximated by

$$[B] = \frac{[A][M]_0}{K_S} \qquad \text{(A6)}$$

Hence, the mass balance equation becomes

$$[A]_0 = [A]\left(1 + \frac{[M]_0}{K_S}\right) + [C] \qquad \text{(A7)}$$

Substitution of eqs A7 and A6 into eq A5 leads to

$$\frac{d[C]}{dt} = k_1\frac{[A]_0[M]_0}{K_S + [M]_0} - \left(\frac{k_1[M]_0}{K_S + [M]_0} + k_{-1}\right)[C] \qquad \text{(A8)}$$

$$k_{obs} = \frac{k_1[M]_0}{K_S + [M]_0} + k_{-1} \qquad \text{(A9)}$$

Observed k_{obs} values as measured by stopped-flow depend linearly on $[M]_0$ (Figure 3C). This would require that K_S be $\gg[M]_0$ if the mechanism given in eq A1 holds true. Thus, eq A9 reduces to

$$k_{obs} = \frac{k_1}{K_S}[M]_0 + k_{-1} = k_{eff}[M]_0 + k_{-1} \qquad \text{(A10)}$$

Therefore, the k_{eff} values given in Table 1 are apparent bimolecular constants, whereas the observed process itself is rate-limited by the C−C ligation step. Empirically, the ratio $k_{eff}^{WT}/k_{eff}^{Var}$ is found to be 24, while it theoretically reflects

$$\frac{k_{eff}^{WT}}{k_{eff}^{Var}} = \frac{k_1^{WT}K_S^{Var}}{k_1^{Var}K_S^{WT}} \qquad \text{(A11)}$$

On the other hand, thermodynamic binding measurements mentioned above yield

$$\frac{K_{app}^{Var}}{K_{app}^{WT}} = \left(\frac{K_S^{Var}K_1^{Var}}{K_S^{WT}K_1^{WT}}\right)\left(\frac{1 + K_1^{WT}}{1 + K_1^{Var}}\right) = 21.2 \qquad \text{(A12)}$$

Both ratios are almost identical. This can be explained by assuming $k_1^{WT} \approx k_1^{Var}$ and $k_{-1}^{WT} \approx k_{-1}^{Var}$. The latter identity is further substantiated by the comparison of the empirical k_{off} values in Table 1 (2.7×10^{-3} and 2.55×10^{-3} s^{-1} for the

wild type and the variant, respectively). So far, kinetic analysis is consistent with the conclusion that the kinetic and thermodynamic effects of pseudophosphorylation are largely due to shifted K_S values.

ACKNOWLEDGMENT

We thank J. Fröbel and K. Schröder-Tittmann for help with the cell fermentation, B. Güttler for technical assistance, and W. Kress for initial kinetic studies on the PDHc-E1 Ser264Glu variant.

SUPPORTING INFORMATION AVAILABLE

Spectroscopic studies on PDHc-E1 Ser264Glu with the pyruvate analogue MAP (Figure 1), additional kinetic NMR studies of pyruvate decarboxylation catalyzed by PDHc-E1 Ser264Glu (Figure 2), and a structural representation of the substrate channel of Ser264Glu showing all common rotamers of the side chain of residue 264 (Figure 3). This material is available free of charge via the Internet at http://pubs.acs.org.

REFERENCES

1. Patel, M. S., and Roche, T. E. (1990) Molecular biology and biochemistry of pyruvate dehydrogenase complexes, *FASEB J. 4*, 3224−3233.
2. Perham, R. N., Milne, J. S., and Subramaniam, S. (2004) The pyruvate dehydrogenase multienzyme complex, in *Thiamine. Catalytic mechanisms in normal and disease states* (Jordan, F., and Patel, M. S., Eds.) pp 331−342, Dekker, New York.
3. Zhou, Z. H., McCarthy, D. B., O'Connor, C. M., Reed, L. J., and Stoops, J. K. (2001) The remarkable structural and functional organization of the eukaryotic pyruvate dehydrogenase complexes, *Proc. Natl. Acad. Sci. U.S.A. 98*, 14802−14807.
4. Patel, M. S., and Korotchkina, L. G. (2006) Regulation of the pyruvate dehydrogenase complex, *Biochem. Soc. Trans. 34*, 217−222.
5. Korotchkina, L. G., and Patel, M. S. (2001) Probing the mechanism of inactivation of human pyruvate dehydrogenase by phosphorylation of three sites, *J. Biol. Chem. 276*, 5731−5738.
6. Ciszak, E. M., Korotchkina, L. G., Dominiak, P. M., Sidhu, S., and Patel, M. S. (2003) Structural basis for flip-flop action of thiamin pyrophosphate-dependent enzymes revealed by human pyruvate dehydrogenase, *J. Biol. Chem. 278*, 21240−21246.
7. Roche, T. E., and Reed, L. J. (1972) Function of the nonidentical subunits of mammalian pyruvate dehydrogenase, *Biochem. Biophys. Res. Commun. 48*, 840−846.
8. Walsh, D. A., Cooper, R. H., Denton, R. M., Bridges, B. J., and Randle, P. J. (1976) The elementary reactions of the pig heart pyruvate dehydrogenase complex. A study of the inhibition by phosphorylation, *Biochem. J. 157*, 41−67.
9. Wynn, R. M., Kato, M., Machius, M., Chuang, J. L., Li, J., Tomchick, D. R., and Chuang, D. T. (2004) Molecular mechanism for regulation of the human mitochondrial branched-chain α-ketoacid dehydrogenase complex by phosphorylation, *Structure 12*, 2185−2196.
10. Seifert, F., Golbik, R., Brauer, J., Lilie, H., Schröder-Tittmann, K., Hinze, E., Korotchkina, L. G., Patel, M. S., and Tittmann, K. (2006) Direct kinetic evidence for half-of-the-sites reactivity in E1 component of human pyruvate dehydrogenase multienzyme complex through alternating sites cofactor activation, *Biochemistry 45*, 12775−12785.
11. Liu, S., Gong, X., Yan, X., Peng, T., Baker, J. C., Li, L., Robben, P. M., Ravindran, S., Andersson, L. A., Cole, A. B., and Roche, T. E. (2001) Reaction mechanism for mammalian pyruvate dehydrogenase using natural lipoyl domain substrates, *Arch. Biochem. Biophys. 386*, 123−135.
12. Kluger, R., and Pike, D. C. (1977) Active site generated analogs of reactive intermediates in enzymic reactions. Potent inhibition of pyruvate dehydrogenase by a phosphonate analog of pyruvate, *J. Am. Chem. Soc. 99*, 4505−4506.
13. Nemeria, N., Baykal, A., Joseph, E., Zhang, S., Yan, Y., Furey, W., and Jordan, F. (2004) Tetrahedral intermediates in thiamin diphosphate-dependent decarboxylations exist as a 1′,4′-imino tautomeric form of the coenzyme, unlike the Michaelis complex or the free coenzyme, *Biochemistry 43*, 6565−6575.
14. Wille, G., Meyer, D., Steinmetz, A., Hinze, E., Golbik, R., and Tittmann, K. (2006) The catalytic cycle of a thiamin diphosphate enzyme examined by cryocrystallography, *Nat. Chem. Biol. 2*, 324−328.
15. Arjunan, P., Sax, M., Brunskill, A., Chandrasekhar, K., Nemeria, N., Zhang, S., Jordan, F., and Furey, W. (2006) A thiamin-bound, pre-decarboxylation reaction intermediate analogue in the pyruvate dehydrogenase E1 subunit induces large scale disorder-to-order transformations in the enzyme and reveals novel structural features in the covalently bound adduct, *J. Biol. Chem. 281*, 15296−15303.
16. Kern, D., Kern, G., Neef, H., Tittmann, K., Killenberg-Jabs, M., Wikner, C., Schneider, G., and Hübner, G. (1997) How thiamine diphosphate is activated in enzymes, *Science 275*, 67−70.
17. Tittmann, K., Golbik, R., Uhlemann, K., Khailova, L., Schneider, G., Patel, M. S., Jordan, F., Chipman, D. M., Duggleby, R. G., and Hübner, G. (2003) NMR analysis of covalent intermediates in thiamin diphosphate enzymes, *Biochemistry 42*, 7885−7891.
18. Ciszak, E., Korotchkina, L. G., Hong, Y. S., Joachimiak, A., and Patel, M. S. (2001) Crystallization and initial X-ray diffraction analysis of human pyruvate dehydrogenase, *Acta Crystallogr. D57*, 565−568.
19. Otwinowski, Z., and Minor, W. (1997) Processing of X-ray diffraction data collected in oscillation mode, *Methods Enzymol. 276*, 307−326.
20. Brunger, A. T., Adams, P. D., Clore, G. M., DeLano, W. L., Gros, P., Grosse-Kunstleve, R. W., Jiang, J. S., Kuszewski, J., Nilges, M., Pannu, N. S., Read, R. J., Rice, L. M., Simonson, T., and Warren, G. L. (1998) Crystallography and NMR System (CNS): A new software package for macromolecular structure determination, *Acta Crystallogr. D54*, 905−921.
21. McRee, D. E. (1999) XtalView/Xfit: A versatile program for manipulating atomic coordinates and electron density, *J. Struct. Biol. 125*, 156−165.
22. Schowen, R. L. (1998) Thiamin-dependent enzymes, in *Comprehensive Biological Catalysis* (Sinnot, M., Ed.) Vol. 2, pp 217−266, Academic Press, London.
23. Frank, R. A., Titman, C. M., Pratap, J. V., Luisi, B. F., and Perham, R. N. (2004) A molecular switch and proton wire synchronize the active sites in thiamine enzymes, *Science 306*, 872−876.
24. Lovell, S. C., Word, J. M., Richardson, J. S., and Richardson, D. C. (2000) The penultimate rotamer library, *Proteins: Struct., Funct., Genet. 40*, 389−408.

BI700083Z